Available online at www.sciencedirect.com
SCIENCE DIRECT®
Journal of Solid State Chemistry 177 (2004) 1117–1126
JOURNAL OF SOLID STATE CHEMISTRY
http://elsevier.com/locate/jssc

Synthesis of open-framework iron phosphates, $[C_5N_2H_{14}]_2[Fe_2^{III}F_2(HPO_4)_4]\cdot 2H_2O$ and $[C_5N_2H_{14}][Fe_4^{III}(H_2O)_4F_2(PO_4)_4]$, with one- and three-dimensional structures

Sukhendu Mandal,[a] Mark A. Green,[b] and Srinivasan Natarajan[a,*]

[a] *Framework Solids Laboratory, Chemistry and Physics of Materials Unit, Jawaharlal Nehru Centre for Advanced Scientific Research (JNCASR), Jakkur P.O., Bangalore 560 064, India*

[b] *Davy-Faraday Research Laboratory, The Royal Institution of Great Britain, 21 Albemarle Street, London W1S 4BS, UK*

Received 30 July 2003; received in revised form 10 October 2003; accepted 14 October 2003

Abstract

The hydrothermal syntheses and structures of two new open-framework iron phosphates, $[C_5N_2H_{14}]_2[Fe_2^{III}F_2(HPO_4)_4]\cdot 2H_2O$, **I**, and $[C_5N_2H_{14}][Fe_4^{III}(H_2O)_4F_2(PO_4)_4]$, **II**, are presented. While the structure of **I** consist of FeO_4F_2 octahedra and HPO_4 terahedra linked to form one-dimensional structure, that of **II** consist of $FeO_4(H_2O)_2$, $FeO_4(H_2O)F$, FeO_4F_2 and PO_4 units connected to give rise to a three-dimensional structure. The structure of **I** resembles the naturally occurring mineral tancoite while **II** resembles the iron phosphate, ULM-12, $[C_6N_2H_{14}][Fe_4(PO_4)_2F_2(H_2O)_3]$. Magnetic susceptibility studies indicate anti-ferromagnetic behavior in both the compounds with $T_N = 200$ and 175 K for **I** and **II**, respectively. Crystal data: **I**, monoclinic, space group $= P2_1/n$ (no. 14). $a = 7.2261(6)$, $b = 16.5731(14)$, $c = 11.0847(10)$ Å, $\beta = 97.265(2)^\circ$, $V = 1316.8(2)$ Å^3, $Z = 4$, $\rho_{calc} = 1.952\,g\,cm^{-1}$, $\mu_{(MoK\alpha)} = 1.446\,mm^{-1}$, $R_1 = 0.0448$ and $wR_2 = 0.1141$ for 1882 data $[I > 2\sigma(I)]$; for **II**, monoclinic, space group $= P2_1/n$ (no. 14). $a = 9.9691(3)$, $b = 12.4013(3)$, $c = 17.3410(3)$ Å, $\beta = 103.762(1)^\circ$, $V = 2082.32(9)$ Å^3, $Z = 4$, $\rho_{calc} = 2.576\,g\,cm^{-1}$, $\mu_{(MoK\alpha)} = 3.162\,mm^{-1}$, $R_1 = 0.0510$ and $wR_2 = 0.1064$ for 2979 data $[I > 2\sigma(I)]$.

Keywords: Hydrothermal synthesis; Iron phosphates; Anti-ferromagnetic

1. Introduction

Naturally occurring iron phosphate minerals exhibit a variety of compositions and structural diversity [1]. Synthetic analogues, on the other hand, is being investigated vigorously during the last decade or so resulting in the isolation of a large number of new iron phosphates with interesting structures [2–31]. One of the compelling reasons for the continued interest in iron phosphates is the possibility of investigating the interplay of structure, dimensionality and magnetism. Thus, iron phosphates with one- [3–6], two- [7–15] and three-dimensional [16–31] structures have been synthesized and characterized.

Most of the open-framework iron phosphates are, in general, synthesized employing hydrothermal methods starting from simple salts of iron, such as chloride or nitrate, in the presence of phosphoric acid and an organic amine. Recently, it was shown that the use of metal complexes in the synthesis mixture provides a facile method for the preparation of new types of open-framework phosphates with novel structures [32]. The use of metal complexes in the synthesis mixture, probably, releases the metal ions slowly in to the solution during the hydrothermal crystallization, thereby facilitating the formation of new structures. We have employed this approach beneficially for the preparation of new iron phosphates with novel structures [16–19]. In continuation of this theme, we have now prepared two new iron phosphates, $[C_5N_2H_{14}]_2[Fe_2^{III}F_2(HPO_4)_4]\cdot 2H_2O$,**I**, and $[C_5N_2H_{14}][Fe_4^{III}(H_2O)_4F_2(PO_4)_4]$, **II**, with one- and

*Corresponding author. Fax: +91-80-846-2766.
E-mail address: raj@jncasr.ac.in (S. Natarajan).

0022-4596/$ - see front matter © 2003 Elsevier Inc. All rights reserved.
doi:10.1016/j.jssc.2003.10.019

three-dimensional structure in the presence of 1,4-diazacycloheptane (homopiperazine, shown below). Whilst **I** has the tancoite structure [33], **II** has a structure closely related to the iron phosphate, $[C_6N_2H_{14}]_2[Fe_4(H_2O)_3F_2(PO_4)_4]$, designated as ULM-12 [22,23].

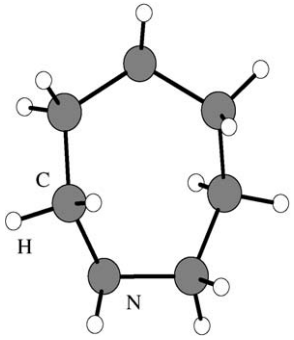

2. Experimental

The title compounds were synthesized under hydrothermal conditions starting from $Fe(OH)_3$ and a coordination complex of Fe^{3+}, $[Fe(acac)_3]$ as the source of iron for **I** and **II**, respectively. In a typical synthesis of **I**, 0.06 g of $Fe(OH)_3$ was dispersed in a mixture of 2 mL of deionized water and 1 mL of 1,4-dioxane. To this 0.07 mL of H_3PO_4 (85 wt%) and 0.08 mL of HF (48% w/w) was added under continuous stirring. Finally, 0.222 g of 1,4-diazacycloheptane (homopiperazine) was added to the above and the mixture was homogenized for 20 min at room temperature. The final brown colored liquid with the composition, $Fe(OH)_3$: $2H_3PO_4$: 4homopiperazine : 4HF : $200H_2O$:21 1,4-dioxane, was transferred and sealed in a 7 mL PTFE-lined stainless steel acid-digestion bomb and heated at 150°C for 96 h. The resulting product, a mixture of black powder and few colorless crystals, were vacuum filtered and washed with plenty of deionized water and dried at ambient conditions. The single crystals could be easily separated from the powder under a polarizing microscope. The black powder was found to be amorphous. Modifications of the above synthesis procedure to prepare **I** in pure form were not successful. The single crystals were separated from the bulk using ultrasonification and used for all other characterizations. For the preparation of **II**, $Fe(acac)_3$ was used instead of $Fe(OH)_3$. Typically, 0.198 g of $Fe(acac)_3$ was dispersed in a mixture of 2 mL of deionized water and 1 mL of buntan-2-ol. To this, 0.14 mL of H_3PO_4 (85 wt%) and 0.08 mL of HF (48% w/w) were added under continuous stirring. Finally, 0.166 g of homopiperazine was added and the mixture was homogenized for 20 min at room temperature. The final orange colored liquid with the composition, $Fe(acac)_3$:$4H_3PO_4$:3homopiperazine:4HF:$200H_2O$:20 butan-2-ol, was transferred and sealed in a 7 mL PTFE-lined stainless steel acid-digestion bomb and heated at 180°C for 72 h. The resulting product contained colorless crystals, were vacuum filtered and washed with plenty of deionized water and dried at ambient conditions. The initial and final pH of the reaction mixture was ~4 in both the cases. The yield of the crystals for **I** and **II** were 50% and 70%, respectively, based on Fe.

3. Single-crystal structure determination

A suitable colorless single crystal of each compound was carefully selected under a polarizing microscope and glued to a thin glass fiber with cyanoacrylate (superglue) adhesive. Crystal structure determination by X-ray diffraction was performed on a Siemen's SMART-CCD diffractometer equipped with a normal focus, 2.4 kW sealed tube X-ray source (Mo$K\alpha$ radiation, $\lambda = 0.71073$ Å) operating at 40 kV and 40 mA. A hemisphere of intensity data were collected at room temperature in 1321 frames with ω scans (width of 0.30° and exposure time of 10 s per frame) in the 2θ range of 3–46.5°. Pertinent experimental details for the structure determinations of **I** and **II** are presented in Table 1.

An absorption correction based on symmetry equivalent reflections was applied using SADABS program [34]. Other effects, such as absorption by the glass fiber, were simultaneously corrected. The structures were solved and refined by SHELXTL-PLUS suite of programs [35]. The direct methods solution readily revealed sufficient fragments of the structure (Fe, P and O) and enabled the remainder of the non-hydrogen atoms to be located from difference Fourier maps. All the hydrogen positions were initially located in the difference map and for the final refinement the hydrogen atoms were placed geometrically and held in the riding mode. Final residuals of $R_1 = 0.04$ and $wR_2 = 0.11$ for **I**, $R_1 = 0.051$ and $wR_2 = 0.106$ for **II**, respectively, were obtained for refinements with varying atomic positions for all the atoms and anisotropic thermal parameters for all non-hydrogen atoms and isotropic thermal parameters for all the hydrogen atoms. Full-matrix least-squares structure refinement against $|F^2|$ was carried out using the SHELXTL-PLUS [35] package of program. The final atomic coordinates, and selected bond distances for **I** are presented in Tables 2 and 3 and the atomic coordinates, and selected bond distances and angles for **II** in Tables 4–6.

4. Results

4.1. $[C_5N_2H_{14}]_2[Fe_2^{III}F_2(HPO_4)_4]\cdot 2H_2O$, **I**

The asymmetric unit of **I** contains 21 non-hydrogen atoms, of which 13 atoms belong to the framework

Table 1
Summary of crystal data, intensity measurements and structure refinements parameters for **I**, $[C_5N_2H_{14}]_2[Fe_2^{III}F_2(HPO_4)_4]\cdot 2H_2O$, and **II**, $[C_5N_2H_{14}][Fe_4^{III}(H_2O)_4F_2(PO_4)_4]$

Parameter	**I**	**II**
Empirical formula	$C_5H_{18}F_1Fe_1N_2O_9P_2$	$C_5H_{22}F_2Fe_4N_2O_{20}P_4$
Crystal system	Monoclinic	Monoclinic
Space group	$P2_1/n$ (no. 14)	$P2_1/n$ (no. 14)
Crystal size (mm)	$0.24\times0.16\times0.16$	$0.12\times0.08\times0.08$
a (Å)	7.2261(6)	9.9691(3)
b (Å)	16.5731(14)	12.4013(3)
c (Å)	11.0847(10)	17.3410(3)
β (deg)	97.265(2)	103.762(1)
Volume (Å^3)	1316.8(2)	2082.32(9)
Z	4	4
Formula mass	387	815.46
ρ_{calc} (g cm^{-3})	1.952	2.576
λ (Mo$K\alpha$) (Å)	0.71073	0.71073
μ (mm^{-1})	1.446	3.162
2θ range (deg)	2.22–23.28	2.04–23.31
Total data collected	5419	8404
Index ranges	$-8\leqslant h\leqslant 7$, $-18\leqslant k\leqslant 17$, $-9\leqslant l\leqslant 12$	$-9\leqslant h\leqslant 11$, $-13\leqslant k\leqslant 13$, $-19\leqslant l\leqslant 17$
Unique data	1882	2979
Observed data ($I>2\sigma(I)$)	1503	2194
Refinement method	Full-matrix least-squares on $\lvert F^2\rvert$	Full-matrix least-squares on $\lvert F^2\rvert$
R_{merg}	0.0351	0.0631
R indexes [$I>2\sigma(I)$]	$R_1=0.0448$;[a] w$R_2=0.1141$[b]	$R_1=0.0510$;[a] w$R_2=0.1064$[b]
R (all data)	$R_1=0.0583$; w$R_2=0.1237$	$R_1=0.0831$; w$R_2=0.1199$
Goodness of fit ($S_{obs.}$)	1.030	1.051
No. of variables	188	334
Largest difference map peak and hole (e Å^{-3})	0.902 and –0.999	1.742 and –1.156

$w=1/[\sigma^2(F_o)^2+(aP)^2+bP]$, $P=[\max.(F_o^2,0)+2(F_c)^2]/3$, where $a=0.0589$ and $b=5.5721$ for **I** and $a=0.0399$ and $b=18.013$ for **II**.
[a] $R_1=\sum||F_o|-|F_c||/\sum|F_o|$.
[b] $wR_2=\{\sum[w(F_o^2-F_c^2)^2]/\sum[w(F_o^2)^2]\}^{1/2}$.

Table 2
Final atomic coordinates ($\times10^4$) and equivalent isotropic displacement parameters (Å $\times10^3$) for **I**, $[C_5N_2H_{14}]_2[Fe_2^{III}F_2(HPO_4)_4]\cdot 2H_2O$

Atom	x	y	z	U_{eq}[a]
Fe(1)	0	5000	5000	14(1)
Fe(2)	5000	5000	5000	16(1)
P(1)	2141(2)	4221(1)	2795(1)	19(1)
P(2)	2167(2)	6390(1)	3690(1)	18(1)
F(1)	2639(4)	4859(2)	5720(2)	20(1)
O(2)	541(5)	4466(2)	3494(3)	24(1)
O(3)	609(5)	6078(2)	4391(3)	25(1)
O(4)	4030(5)	5995(2)	4198(3)	27(1)
O(5)	4016(5)	4317(2)	3600(3)	29(1)
O(6)	1878(6)	3383(2)	2325(4)	36(1)
O(7)	2132(6)	4799(2)	1672(3)	36(1)
O(8)	1740(6)	6293(2)	2343(3)	34(1)
O(9)	2331(6)	7300(2)	4067(3)	30(1)
O(100)	−1898(7)	5904(4)	801(5)	72(2)
N(1)	7898(7)	8606(3)	2358(5)	33(1)
C(1)	8122(8)	7728(3)	2159(5)	29(1)
C(2)	6726(8)	7205(4)	2675(6)	32(1)
N(2)	7330(11)	7685(5)	4861(6)	78(2)
C(3)	7194(7)	7004(3)	3989(4)	14(1)
C(4)	8290(20)	8378(5)	4627(8)	122(5)
C(5)	8101(10)	8924(4)	3653(6)	50(2)

[a] U_{eq} is defined as one-third of the trace of the orthogonalized U_{ij} tensor.

and 8 atoms to the guest species, which include one homopiperazine and a water molecule. There are two crystallographically independent Fe and P atoms. The iron atoms, Fe(1) and Fe(2), occupies special position with a site occupancy (SOF) of 0.5. Each iron atom bonds with 4 oxygen and 2 fluorine atoms forming an octahedral with average Fe–O/F distances of 1.977 Å. The O/F–Fe–O/F bond angles are nearly octahedral and show a deviation of only $\pm3°$ from the ideal value of 90° and 180° for the in plane and out-of-plane angles. The iron atom makes four Fe–O–P linkages to the two distinct P atom neighbors with an average Fe–O–P bond angle of 138.03°. The iron atoms are connected through the fluorine atoms forming infinite Fe–F–Fe one-dimensional chains. Each phosphorous atom makes two P–O–Fe bond and possess two terminal P–O linkages. The P–O distances are in the range 1.487(4)–1.570(4) Å (av. P–O = 1.531) and the O–P–O bond angles are in the range 102.9(2)–113.4(2)° (av. 109.4°). The terminal P(1)–O(7) and P(2)–O(9) bonds with distances of 1.570(4) and 1.565(4) Å are formally P–OH linkages. One hydrogen position near each of the oxygen atoms O(7) and O(9) was observed in the difference Fourier maps. The other two terminal bonds, P(1)–O(6) and P(2)–O(8), with distances of 1.487(4) and

Table 3
Selected bond distances (Å) and angles (deg) for **I**, $[C_5N_2H_{14}]_2[Fe_2^{III}F_2(HPO_4)_4]\cdot 2H_2O$

Bond	Distance (Å)	Bond	Distance (Å)
Fe(1)–O(2)	1.972(3) [0.562]	Fe(2)–F(1)	1.987(3) [0.435]
Fe(1)–O(2)#1	1.972(3) [0.562]	**Σ (Fe–O)**	**[3.132]**
Fe(1)–O(3)#1	1.980(3) [0.550]	P(1)–O(6)	1.487(4) [1.421]
Fe(1)–O(3)	1.980(3) [0.550]	P(1)–O(2)	1.526(4) [1.279]
Fe(1)–F(1)	1.986(3) [0.436]	P(1)–O(5)	1.533(4) [1.255]
Fe(1)–F(1)#1	1.986(3) [0.436]	P(1)–O(7)	1.570(4) [1.135]
Σ (Fe–O)	**[3.046]**	**Σ (P–O)**	**[5.09]**
Fe(2)–O(4)	1.961(4) [0.579]	P(2)–O(8)	1.495(4) [1.391]
Fe(2)–O(4)#2	1.961(4) [0.579]	P(2)–O(3)	1.536(4) [1.245]
Fe(2)–O(5)#2	1.979(4) [0.552]	P(2)–O(4)	1.538(4) [1.238]
Fe(2)–O(5)	1.979(4) [0.552]	P(2)–O(9)	1.565(4) [1.151]
Fe(2)–F(1)#2	1.987(3) [0.435]	**Σ (P–O)**	**[5.025]**
Angle	Amplitude (deg)	Angle	Amplitude (deg)
O(2)–Fe(1)–O(2)#1	180.00(19)	O(5)–Fe(2)–F(1)#2	89.62(13)
O(2)–Fe(1)–O(3)#1	87.71(15)	O(4)–Fe(2)–F(1)	90.30(13)
O(2)#1–Fe(1)–O(3)#1	92.29(15)	O(4)#2–Fe(2)–F(1)	89.70(13)
O(2)–Fe(1)–O(3)	92.29(15)	O(5)#2–Fe(2)–F(1)	89.62(13)
O(2)#1–Fe(1)–O(3)	87.71(15)	O(5)–Fe(2)–F(1)	90.38(13)
O(3)#1–Fe(1)–O(3)	179.999(1)	F(1)#2–Fe(2)–F(1)	179.998(1)
O(2)–Fe(1)–F(1)	90.26(13)	O(6)–P(1)–O(2)	110.8(2)
O(2)#1–Fe(1)–F(1)	89.74(13)	O(6)–P(1)–O(5)	111.4(2)
O(3)#1–Fe(1)–F(1)	90.01(13)	O(2)–P(1)–O(5)	110.3(2)
O(3)–Fe(1)–F(1)	89.98(13)	O(6)–P(1)–O(7)	107.7(2)
O(2)–Fe(1)–F(1)#1	89.74(13)	O(2)–P(1)–O(7)	108.2(2)
O(2)#1–Fe(1)–F(1)#1	90.26(13)	O(5)–P(1)–O(7)	108.3(2)
O(3)#1–Fe(1)–F(1)#1	89.99(13)	O(8)–P(2)–O(3)	113.4(2)
O(3)–Fe(1)–F(1)#1	90.01(13)	O(8)–P(2)–O(4)	112.3(2)
F(1)–Fe(1)–F(1)#1	180.0	O(3)–P(2)–O(4)	109.6(2)
O(4)–Fe(2)–O(4)#2	180.00(12)	O(8)–P(2)–O(9)	111.8(2)
O(4)–Fe(2)–O(5)#2	86.95(16)	O(3)–P(2)–O(9)	102.9(2)
O(4)#2–Fe(2)–O(5)#2	93.05(16)	O(4)–P(2)–O(9)	106.2(2)
O(4)–Fe(2)–O(5)	93.05(16)	Fe(1)–F(1)–Fe(2)	130.87(14)
O(4)#2–Fe(2)–O(5)	86.95(16)	P(1)–O(2)–Fe(1)	142.5(2)
O(5)#2–Fe(2)–O(5)	180.000(1)	P(2)–O(3)–Fe(1)	133.2(2)
O(4)–Fe(2)–F(1)#2	89.70(13)	P(2)–O(4)–Fe(2)	140.4(2)
O(4)#2–Fe(2)–F(1)#2	90.30(13)	P(1)–O(5)–Fe(2)	136.0(2)
O(5)#2–Fe(2)–F(1)#2	90.38(13)		

Symmetry transformations used to generate equivalent atoms: #1, $-x,-y+1,-z+1$; #2, $-x+1,-y+1,-z+1$.

1.495(4) are P=O linkages. The various bond distances and bond angles observed in **I** are similar to those observed in other phosphate based open-framework solids [2–31]. Bond valence sum (BVS) calculations [36] also agree with the above and clearly indicate that the iron atoms are in +3 state. The complete list of bond distances along with BVS values for **I** is presented in Table 3.

The structure of **I** is built up from isolated infinite $\{[FeF(HPO_4)_2]^{2-}\}_\infty$ chains running in the *ab* plane (Fig. 1a). The diprotonated homopiperazine along with the water molecules occupy the inter-chain spaces and interact with the chains through hydrogen bonds (Fig. 1b). Each $\{[FeF(HPO_4)_2]^{2-}\}_\infty$ chain is built up from a chain of $Fe^{III}O_4F_2$ octahedra linked by their *trans* fluorine atoms. The HPO_4 tetrahedra are grafted onto this chain such that each iron octahedron shares its four oxygen atoms with four distinct phosphorous tetrahedra. Similar connectivity involving the octahedral and tetrahedral units has been encountered in many mineralogical structure related to tancoite [33]. The projection of the structure down the chain axis, showing the layout of adjacent chains is given in Fig. 2. It may be noted that strong intra- and inter-chain hydrogen bond interactions exist between the adjacent chains, through the terminal hydroxyl groups. Such hydrogen bond interactions, probably, lend additional structural stability in **I**. The complete list of the hydrogen bond interactions is listed in Table 7.

4.2. $[C_5N_2H_{14}][Fe_4^{III}(H_2O)_4F_2(PO_4)_4]$, *II*

The asymmetric unit contains 37 non-hydrogen atoms, of which 30 atoms belong to the framework

Table 4
Final atomic coordinates ($\times 10^4$) and equivalent isotropic displacement parameters (Å $\times 10^3$) for **II**, $[C_5N_2H_{14}][Fe_4^{III}(H_2O)_4F_2(PO_4)_4]$

Atom	x	y	z	U_{eq}[a]
Fe(1)	8664(1)	3534(1)	−761(1)	12(1)
Fe(2)	12,453(1)	4221(1)	−2203(1)	10(1)
Fe(3)	14,403(1)	4739(1)	−3692(1)	11(1)
Fe(4)	9707(1)	6098(1)	−2920(1)	11(1)
P(1)	10,843(2)	5407(2)	−1067(1)	10(1)
P(2)	15,619(2)	3726(2)	−1920(1)	10(1)
P(3)	12,803(2)	6545(2)	−2957(1)	11(1)
P(4)	13,036(2)	4121(2)	−5582(1)	11(1)
O(1)	8399(6)	2083(5)	−434(4)	20(2)
O(2)	8581(6)	4008(5)	287(3)	20(2)
O(3)	6826(6)	4053(5)	−1222(3)	14(1)
O(4)	9475(6)	4850(5)	−1036(4)	20(2)
O(5)	10,784(8)	2918(7)	−557(5)	55(2)
O(6)	8815(10)	2897(6)	−1894(5)	63(3)
O(7)	14,293(6)	3825(4)	−1621(3)	12(1)
O(8)	11,893(6)	4547(5)	−1196(3)	14(1)
F(9)	12,859(5)	4082(4)	−3274(3)	14(1)
O(10)	11,759(6)	2697(4)	−2299(3)	14(1)
F(11)	10,519(5)	4609(4)	−2793(3)	14(1)
O(12)	13,104(6)	5785(5)	−2239(3)	14(1)
O(13)	16,054(6)	5363(5)	−3940(3)	18(2)
O(14)	13,203(6)	4689(5)	−4783(3)	15(1)
O(15)	13,692(6)	6195(5)	−3542(3)	15(1)
O(16)	15,582(6)	4509(5)	−2605(3)	13(1)
O(17)	14,970(6)	3160(5)	−3911(3)	17(2)
O(18)	9126(6)	7583(5)	−2829(3)	15(1)
O(19)	11,253(6)	6489(5)	−3378(4)	14(1)
O(20)	8488(6)	5783(5)	−3977(3)	19(2)
O(21)	10,556(6)	6234(4)	−1739(3)	12(1)
O(22)	8040(6)	5575(5)	−2477(4)	23(2)
N(1)	15,237(14)	1575(10)	401(7)	79(4)
C(1)	13,811(15)	1546(10)	265(13)	103(8)
C(2)	13,470(20)	2060(14)	1047(15)	139(10)
C(3)	13,296(13)	3256(11)	1003(12)	86(6)
N(2)	14,452(12)	3908(10)	955(10)	105(6)
C(4)	15,340(20)	3616(11)	471(10)	96(7)
C(5)	16,031(13)	2588(12)	546(9)	62(4)

[a] U_{eq} is defined as one-third of the trace of the orthogonalized U_{ij} tensor.

Table 5
Selected bond distances (Å) in **II**, $[C_5N_2H_{14}][Fe_4^{III}(H_2O)_4F_2(PO_4)_4]$

Bond	Distance (Å)	Bond	Distance (Å)
Fe(1)–O(1)	1.924(6) [0.640]	Fe(4)–F(11)	2.007(5) [0.412]
Fe(1)–O(3)	1.927(6) [0.635]	Fe(4)–O(21)	2.028(6) [0.483]
Fe(1)–O(2)	1.930(6) [0.630]	Fe(4)–O(22)	2.093(6) [0.405]
Fe(1)–O(4)	1.931(6) [0.628]	**Σ (Fe–O)**	**[3.035]**
Fe(1)–O(6)	2.157(8) [0.341]	P(1)–O(2)#1	1.522(6) [1.293]
Fe(1)–O(5)	2.196(8) [0.307]	P(1)–O(21)	1.527(6) [1.275]
Σ (Fe–O)	**[3.181]**	P(1)–O(4)	1.540(6) [1.231]
Fe(2)–O(7)	1.934(5) [0.623]	P(1)–O(8)	1.548(6) [1.205]
Fe(2)–O(8)	1.997(6) [0.526]	**Σ (P–O)**	**[5.004]**
Fe(2)–F(9)	2.001(5) [0.419]	P(2)–O(18)#2	1.522(6) [1.293]
Fe(2)–O(10)	2.006(6) [0.513]	P(2)–O(16)	1.528(6) [1.272]
Fe(2)–F(11)	2.014(5) [0.404]	P(2)–O(7)	1.536(6) [1.245]
Fe(2)–O(12)	2.052(6) [0.453]	P(2)–O(3)#3	1.544(6) [1.218]
Σ (Fe–O)	**[2.938]**	**Σ (P–O)**	**[5.028]**
Fe(3)–O(13)	1.957(6) [0.586]	P(3)–O(10)#4	1.529(6) [1.269]
Fe(3)–O(15)	1.979(6) [0.552]	P(3)–O(12)	1.534(6) [1.251]
Fe(3)–O(14)	1.985(6) [0.543]	P(3)–O(19)	1.545(6) [1.215]
Fe(3)–O(16)	1.991(6) [0.534]	P(3)–O(15)	1.558(6) [1.173]
Fe(3)–F(9)	2.022(5) [0.396]	**Σ (P–O)**	**[4.908]**
Fe(3)–O(17)	2.098(6) [0.400]	P(4)–O(13)#5	1.509(6) [1.339]
Σ (Fe–O)	**[3.010]**	P(4)–O(14)	1.528(6) [1.272]
Fe(4)–O(18)	1.948(6) [0.600]	P(4)–O(20)#6	1.534(6) [1.251]
Fe(4)–O(19)	1.956(6) [0.587]	P(4)–O(1)#7	1.543(6) [1.221]
Fe(4)–O(20)	1.982(6) [0.547]	**Σ (P–O)**	**[5.084]**

Symmetry transformations used to generate equivalent atoms: #1, $-x+2$, $-y+1$, $-z$; #2, $-x+5/2$, $y-1/2$, $-z-1/2$; #3, $x+1$, y, z; #4, $-x+5/2$, $y+1/2$, $-z-1/2$; #5, $-x+3$, $-y+1$, $-z-1$; #6, $-x+2$, $-y+1$, $-z-1$; #7, $x+1/2$, $-y+1/2$, $z-1/2$.

and 7 atoms to the guest molecules. There are four crystallographically independent Fe and P atoms. All the iron atoms are octahedrally coordinated with respect to oxygen and fluorine neighbors. Thus, we have $Fe(1)O_4(H_2O)_2$, $Fe(2)O_4F_2$, $Fe(3)O_4(H_2O)F$ and $F(4)O_4(H_2O)F$ polyhedra with Fe–O/F distances in the range 1.924(6)–2.196(8) Å (av. Fe–O/F = 2.005 Å). The O/F–Fe–O/F bond angles are in the range 75.3(4)–178.7(2)° (av. O/F–Fe(1)–O/F = 105.6, O/F–Fe(2)–O/F = 106.9, O/F–Fe(3)–O/F = 106.4, O/F–Fe(4)–O/F = 106°). All the iron atoms make four Fe–O–P bonds with an average Fe–O–P bond angle of 138.8°. The other two connection needed to complete the octahedra comes from two terminal H_2O molecules for Fe(1), two bridging F atoms for Fe(2), one terminal H_2O molecule and a fluorine bridge for Fe(3) and Fe(4). The average Fe–F–Fe bond angle is 127.8°. All the P atoms make four P–O–Fe linkages. The P–O distances are in the range 1.509(6)–1.558(6) Å (av. P–O = 1.534 Å) and O–P–O bond angles have an average value of 109.5°. The various bond distances and angles observed in **II** are comparable to those reported in the literature [3–31]. BVS calculations, based on Brown and Altermatt [36], indicate the valence states of Fe, P and O to be +3, +5 and −2, respectively. The selected bond distances and angles along with the BVS values for **II** is presented in Tables 5 and 6.

The complex framework structure of **II** can be understood in terms of simpler building units. Thus, the structure of **II**, consists of two types of secondary building units (SBUs). Thus, $Fe(2)O_4F_2$, $Fe(3)O_4(H_2O)F$ and $Fe(4)O_4(H_2O)F$ octahedra are connected to P(1), P(2) and P(3) tetrahedra forming a hexamer unit (SBU-6), $Fe_3(H_2O)_2F_2(PO_4)_3$ (Figs. 3a and b). The three Fe^{III} octahedra are linked together through the corners by F atoms forming a Fe trimer. The PO_4 are grafted on to the Fe-trimer forming the SBU-6 building units. The $Fe(1)O_4(H_2O)_2$ octahedra and $P(4)O_4$ tetrahedra form a simple corner-shared dimer (SBU-2) units. The dimer and the hexamer unit have been identified as one of the basic building units in systems involving octahedral–tetrahedral building units

Table 6
Selected bond angles (deg) in **II**, $[C_5N_2H_{14}][Fe_4^{III}(H_2O)_4F_2(PO_4)_4]$

Angle	Amplitude (deg)	Angle	Amplitude (deg)
O(1)–Fe(1)–O(3)	104.5(3)	O(18)–Fe(4)–O(21)	84.3(2)
O(1)–Fe(1)–O(2)	88.2(3)	O(19)–Fe(4)–O(21)	102.1(2)
O(3)–Fe(1)–O(2)	92.3(3)	O(20)–Fe(4)–O(21)	165.2(2)
O(1)–Fe(1)–O(4)	163.4(3)	F(11)–Fe(4)–O(21)	84.6(2)
O(3)–Fe(1)–O(4)	91.6(2)	O(18)–Fe(4)–O(22)	89.2(2)
O(2)–Fe(1)–O(4)	95.2(3)	O(19)–Fe(4)–O(22)	175.8(3)
O(1)–Fe(1)–O(6)	88.2(3)	O(20)–Fe(4)–O(22)	85.0(2)
O(3)–Fe(1)–O(6)	90.6(3)	F(11)–Fe(4)–O(22)	90.5(2)
O(2)–Fe(1)–O(6)	175.9(3)	O(21)–Fe(4)–O(22)	80.4(2)
O(4)–Fe(1)–O(6)	87.7(3)	O(2)#1–P(1)–O(21)	108.7(3)
O(1)–Fe(1)–O(5)	79.7(3)	O(2)#1–P(1)–O(4)	109.5(4)
O(3)–Fe(1)–O(5)	165.2(3)	O(21)–P(1)–O(4)	108.8(3)
O(2)–Fe(1)–O(5)	102.1(3)	O(2)#1–P(1)–O(8)	109.4(3)
O(4)–Fe(1)–O(5)	83.7(3)	O(21)–P(1)–O(8)	111.3(3)
O(6)–Fe(1)–O(5)	75.3(4)	O(4)–P(1)–O(8)	109.3(3)
O(7)–Fe(2)–O(8)	91.3(2)	O(18)#2–P(2)–O(16)	110.1(3)
O(7)–Fe(2)–F(9)	94.9(2)	O(18)#2–P(2)–O(7)	112.8(3)
O(8)–Fe(2)–F(9)	171.8(2)	O(16)–P(2)–O(7)	110.4(3)
O(7)–Fe(2)–O(10)	94.0(2)	O(18)#2–P(2)–O(3)#3	108.5(3)
O(8)–Fe(2)–O(10)	95.8(2)	O(16)–P(2)–O(3)#3	108.3(3)
F(9)–Fe(2)–O(10)	89.1(2)	O(7)–P(2)–O(3)#3	106.7(3)
O(7)–Fe(2)–F(11)	178.7(2)	O(10)#4–P(3)–O(12)	110.5(3)
O(8)–Fe(2)–F(11)	87.9(2)	O(10)#4–P(3)–O(19)	111.3(3)
F(9)–Fe(2)–F(11)	85.96(19)	O(12)–P(3)–O(19)	109.7(3)
O(10)–Fe(2)–F(11)	85.0(2)	O(10)#4–P(3)–O(15)	106.4(3)
O(7)–Fe(2)–O(12)	89.3(2)	O(12)–P(3)–O(15)	109.0(3)
O(8)–Fe(2)–O(12)	89.5(2)	O(19)–P(3)–O(15)	109.9(3)
F(9)–Fe(2)–O(12)	85.2(2)	O(13)#5–P(4)–O(14)	110.6(3)
O(10)–Fe(2)–O(12)	173.6(2)	O(13)#5–P(4)–O(20)#6	110.3(3)
F(11)–Fe(2)–O(12)	91.7(2)	O(14)–P(4)–O(20)#6	107.3(3)
O(13)–Fe(3)–O(15)	90.9(2)	O(13)#5–P(4)–O(1)#7	110.7(4)
O(13)–Fe(3)–O(14)	98.7(2)	O(14)–P(4)–O(1)#7	108.9(3)
O(15)–Fe(3)–O(14)	90.0(2)	O(20)#6–P(4)–O(1)#7	108.9(4)
O(13)–Fe(3)–O(16)	85.8(2)	P(4)#8–O(1)–Fe(1)	154.1(4)
O(15)–Fe(3)–O(16)	99.0(2)	P(1)#1–O(2)–Fe(1)	152.8(4)
O(14)–Fe(3)–O(16)	169.9(2)	P(2)#9–O(3)–Fe(1)	136.4(4)
O(13)–Fe(3)–F(9)	171.8(2)	P(1)–O(4)–Fe(1)	144.5(4)
O(15)–Fe(3)–F(9)	89.6(2)	P(2)–O(7)–Fe(2)	129.1(3)
O(14)–Fe(3)–F(9)	89.5(2)	P(1)–O(8)–Fe(2)	127.2(3)
O(16)–Fe(3)–F(9)	86.0(2)	Fe(2)–F(9)–Fe(3)	129.6(2)
O(13)–Fe(3)–O(17)	93.0(3)	P(3)#2–O(10)–Fe(2)	141.9(4)
O(15)–Fe(3)–O(17)	174.7(2)	Fe(4)–F(11)–Fe(2)	126.0(2)
O(14)–Fe(3)–O(17)	85.7(2)	P(3)–O(12)–Fe(2)	127.1(3)
O(16)–Fe(3)–O(17)	85.0(2)	P(4)#5–O(13)–Fe(3)	159.3(4)
F(9)–Fe(3)–O(17)	87.1(2)	P(4)–O(14)–Fe(3)	142.2(4)
O(18)–Fe(4)–O(19)	94.4(2)	P(3)–O(15)–Fe(3)	128.1(3)
O(18)–Fe(4)–O(20)	97.6(3)	P(2)–O(16)–Fe(3)	136.7(3)
O(19)–Fe(4)–O(20)	92.4(2)	P(2)#4–O(18)–Fe(4)	141.6(4)
O(18)–Fe(4)–F(11)	168.7(2)	P(3)–O(19)–Fe(4)	128.0(4)
O(19)–Fe(4)–F(11)	86.4(2)	P(4)#6–O(20)–Fe(4)	139.6(4)
O(20)–Fe(4)–F(11)	93.6(2)	P(1)–O(21)–Fe(4)	132.2(3)

Symmetry transformations used to generate equivalent atoms: #1, $-x+2,-y+1,-z$; #2, $-x+5/2,y-1/2,-z-1/2$; #3, $x+1,y,z$; #4, $-x+5/2,y+1/2,-z-1/2$; #5, $-x+3,-y+1,-z-1$; #6, $-x+2,-y+1,-z-1$; #7, $x+1/2,-y+1/2,z-1/2$; #8, $x-1/2,-y+1/2,z+1/2$; #9, $x-1,y,z$.

[37–41]. The hexamer SBU-6 units are connected through 4-membered rings forming a one-dimensional chains and are connected by both the $Fe(1)O_4(H_2O)_2$ units and $P(4)O_4$ as shown independently in Figs. 4a and b. All the connectivity originating from the SBU-2 units is shown in Figs. 5a and b. In Fig. 5a, the connectivity from the $Fe(1)O_4(H_2O)_2$ octahedra and in Fig. 5b the connectivity from the $P(4)O_4$ tetrahedra with the SBU-6 units are shown. The connectivity between the octahedra and tetrahedra gives rise to 8-membered

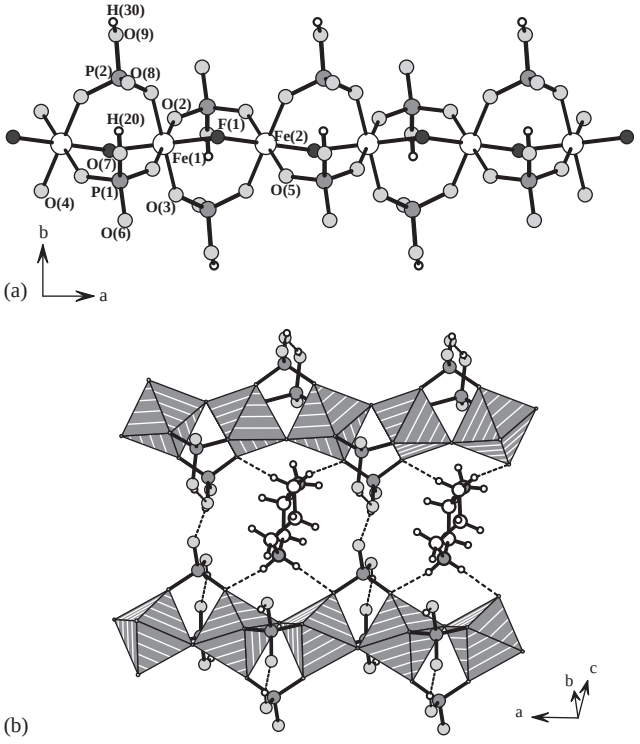

Fig. 1. (a) Structure of **I** in the *ab* plane showing the tancoite chain. (b) Two one-dimensional chains in **I** along with the amine molecules. Dotted lines represent possible hydrogen bond interactions.

Table 7
Important hydrogen bond interactions in **I**, $[C_5N_2H_{14}]_2[Fe_2^{III}F_2(HPO_4)_4]\cdot 2H_2O$, and **II**, $[C_5N_2H_{14}][Fe_4^{III}(H_2O)_4F_2(PO_4)_4]$

D–H···A	D–H (Å)	H···A (Å)	D···A (Å)	D–H···A (deg)
I				
N(1)–H(1)–O(2)	0.90	2.06	2.916(6)	159
N(1)–H(2)–O(5)	0.90	1.96	2.844(6)	167
O(7)–H(20)–O(8)[a]	0.82	1.81	2.611(5)	167
O(9)–H(30)–O(6)[a]	0.82	1.70	2.480(5)	158
O(100)–H(101)–O(7)	1.00	1.97	2.964(7)	165
O(100)–H(102)–O(8)	0.99	2.06	3.019(7)	162
C(1)–H(4)–O(9)	0.97	2.46	3.403(6)	165
C(2)–H(5)–O(6)	0.97	2.31	3.255(7)	163
C(2)–H(6)–O(100)	0.97	2.42	3.237(7)	142
C(3)–H(9)–O(4)	0.97	1.92	2.866(6)	163
C(3)–H(10)–O(3)	0.97	1.93	2.892(6)	174
C(4)–H(12)–O(8)	0.97	2.59	3.387(2)	140
II				
N(1)–H(1)–O(20)	0.90	2.31	3.189(3)	164
N(1)–H(2)–F(9)	0.90	2.46	3.149(3)	134
N(2)–H(9)–O(3)	0.90	2.16	2.918(4)	141
N(2)–H(10)–O(12)	0.90	2.09	2.908(3)	151
C(1)–H(3)–O(14)	0.97	2.16	3.039(5)	150
C(2)–H(6)–F(11)	0.97	2.42	3.468(2)	167
C(3)–H(8)–O(22)	0.97	2.52	3.468(2)	167
C(5)–H(14)–O(1)	0.97	2.35	3.281(2)	160

[a] Intra-chain.

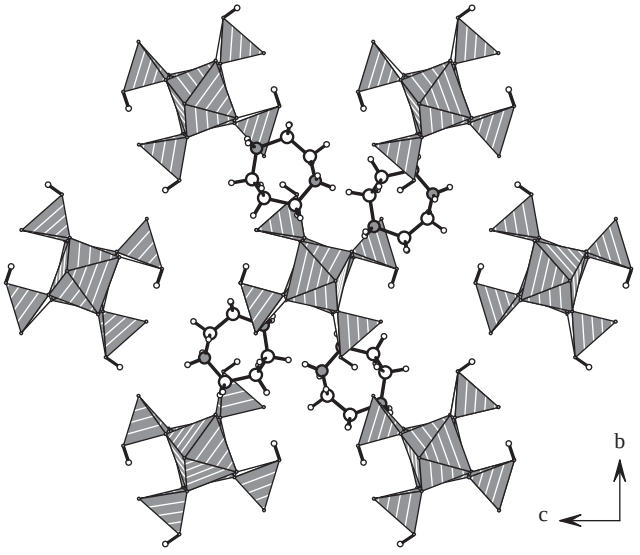

Fig. 2. Structure of **I** in the *bc* plane showing the view down the chain axis. Note that the chains are arranged as a hexagon.

channels (Fig. 6). The amine molecule occupies these channels.

5. Discussion

Two new iron(III) phosphates, **I**, $[C_5N_2H_{14}]_2[Fe_2^{III}F_2(HPO_4)_4]\cdot 2H_2O$, **II**, and $[C_5N_2H_{14}]$

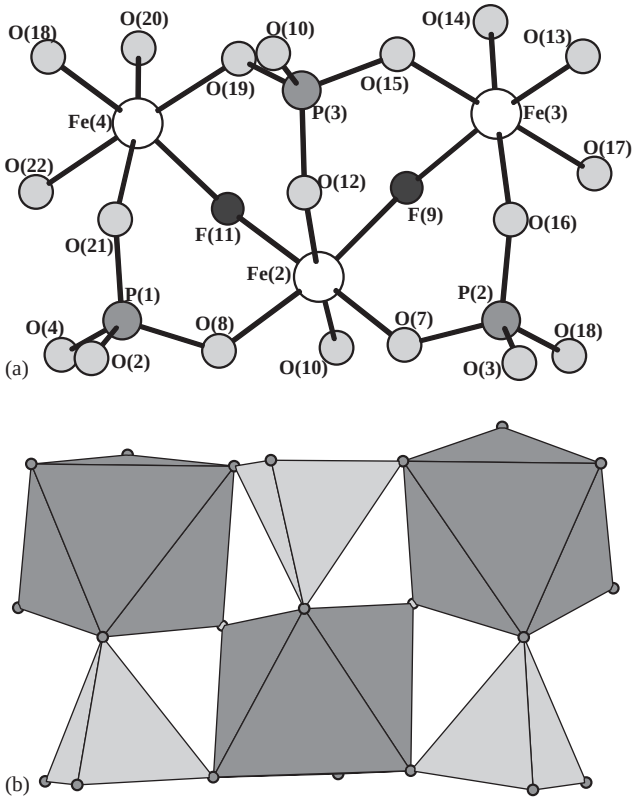

Fig. 3. The hexamer unit observed in **II** (SBU-6) (a) ball and stick view and (b) polyhedral view.

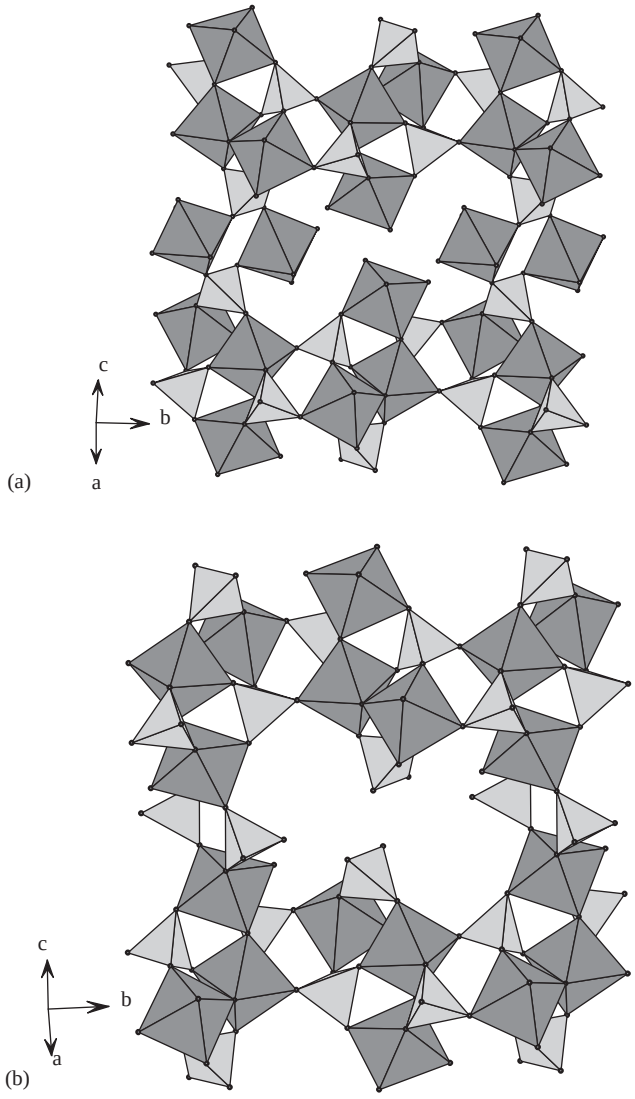

Fig. 4. Structure of **II** showing the connectivity between the hexamer SBU-6 units (a) through the $Fe(1)O_4(H_2O)_2$ octahedra and (b) through the $P(4)O_4$ tetrahedra (hatched octahedra—Fe, gray tetrahedra—P)

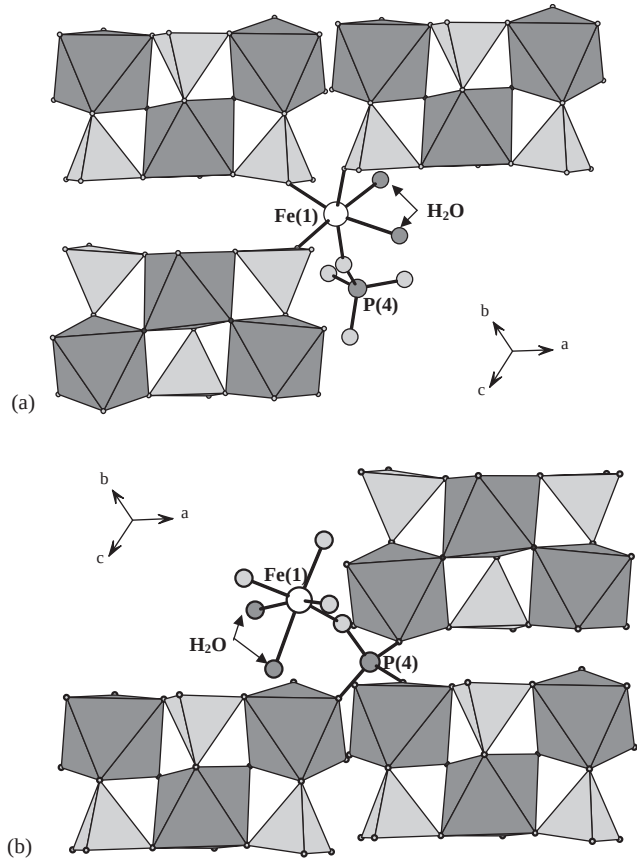

Fig. 5. Structure of **II** showing the connectivity between the hexamer SBU-6 and SBU-2 units (a) through $Fe(1)O_4(H_2O)_2$ octahedral units and (b) through the $P(4)O_4$ tetrahedra. The hatched atoms of the terminal Fe–O linkages are water molecules.

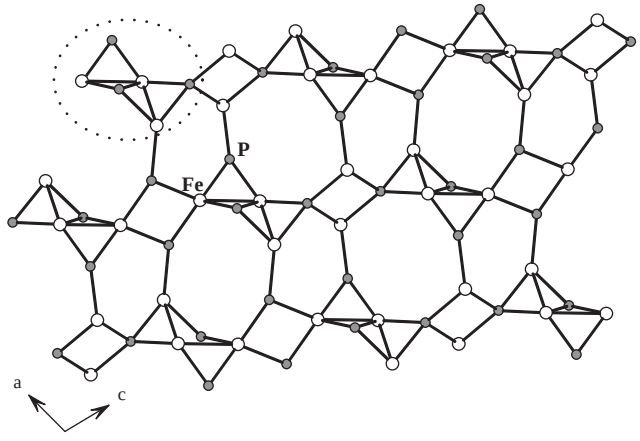

Fig. 6. Fe and P atom connectivity in **II** showing the 8-membered channels in the *ac* plane. Note that the SBU-6 and SBU-2 units are connected through the corners.

$[Fe_4^{III}(H_2O)_4F_2(PO_4)_4]$, have been obtained as good quality single crystals by hydrothermal methods. Whilst **I** is one-dimensional, **II** is three-dimensional in nature. Both the compounds contain Fe in $+3$ oxidation state. Though the compound formula may not be necessarily deducible from the single-crystal X-ray data due to the possibility of non-integer hydrogen occupation [42], we have employed bond-valence sum calculation and magnetic measurements to arrive at the valence state of Fe for both the compounds. Although the structures of both **I** and **II** are formed from the expected polyhedral building units, distinct differences exist between them. Thus, compound **I** is formed from FeO_4F_2 octahedra and HPO_4 terahedra and compound **II** is formed by $Fe(1)O_4(H_2O)_2$, $Fe(2)O_4F_2$, $Fe(3)O_4(H_2O)F$ and $Fe(4)O_4(H_2O)F$ octahedra and PO_4 tetrahedra. While **I** possess infinite one-dimensional chains of Fe–O/F–Fe, only short Fe_3 trimers have been observed in **II**. The linear chains in **I** are formed by the corner sharing of FeO_4F_2 octahedra through the Fe–μ(F)–Fe linkages and Fe_3 trimers in **II**, have been

formed by the corner sharing of Fe–μ(F)–Fe linkage. In addition to the commonality between the structures of **I** and **II**, the structures themselves merit comparison with other known phases possessing similar structural features.

As mentioned earlier, the structure of **I** is similar to that of tancoite. Tancoite is a phosphate mineral of the formula, $LiNa_2HAl(PO_4)_2(OH)$, possessing one-dimensional chain structure, discovered at the Tanco Mine, Bernic Lake, Manitoba [43]. This type of chains has been encountered in many phosphate, sulfate and silicate minerals [33]. The chains generally has the composition, $[M(TO_4)_2L]_n$ (M and T are cations of different coordination, usually octahedral and tetrahedral, L = anionic ligand, e.g., O^{2-}, OH^- or F^-). Iron phosphates with tancoite chains have also been reported in the literature with compositions of $[N_2C_3H_{12}][FeF(HPO_4)_2]\cdot xH_2O$ ($x = 0.2$) (3), $[C_2N_2H_{10}][Fe(OH)(HPO_4)_2]$ (5), $[NH_3(CH_2)_2CH(NH_3)CH_2CH_3][FeF(HPO_4)_2]$ (6) and $[C_6N_2H_{14}][Fe_2F_2(HPO_4)_2(H_2PO_4)_2]\cdot 2H_2O$ (19), prepared in the presence of different amines. It is to be noted that both the phosphate groups in most of these iron phosphates are similar possessing one terminal P–OH linkages, and the difference between the two structures are the way the iron atoms are linked. The iron phosphates generally have Fe atoms linked through a fluoride bridge, in $[C_2N_2H_{10}][Fe(OH)(HPO_4)_2]$ (5) it is through a hydroxyl group. In **I**, we have similar connectivity with the iron atoms being bridged by their corner via a fluoride ion. Similar tancoite chains have also been observed in many of the reported structures of Al and Ga phosphates possessing tancoite chains [44,45].

The structure of **II** is formed by the connectivity involving the $Fe_3(H_2O)_2F_2(PO_4)_3$ hexamer (SBU-6) and a simple SBU-2 dimer. The structure of **II** is similar to the iron phosphate, $Fe_4(PO_4)_4F_2(H_2O)_3\cdot[C_6H_{14}N_2]$, synthesized in the presence of DABCO cations [22,23]. The difference between the two structures being the present compound is formed entirely by octahedral Fe, while $Fe_4(PO_4)_4F_2(H_2O)_3\cdot[C_6H_{14}N_2]$ has a square-pyramidal iron. The presence of octahedral coordination for all the Fe^{3+} ions does not create any observable differences between the two structures.

Magnetic susceptibility has been measured as a function of temperature on powdered single crystals was performed for both the compounds using a SQUID magnetometer using an applied field of 100 Oe. The temperature dependence of the magnetic susceptibility is shown in Figs. 7 and 8. The variation of the inverse susceptibility is shown as an inset. The high temperature magnetic susceptibility data was fitted for Curie–Weiss behavior. The resulting Curie–Weiss temperature ($\theta_p \sim -166$ and -246 K for **I** and **II**) is consistent with the presence of anti-ferromagnetic interactions. The increase in the magnetic susceptibility as low temperature, in the case of **I**, is likely to be due to the presence of a small amount of paramagnetic impurities in the sample. The room temperature magnetic moment obtained from the experimental data (5.76 and 5.92 μ_B, for **I** and **II**, respectively) also indicates that the oxidation state of iron is +3.

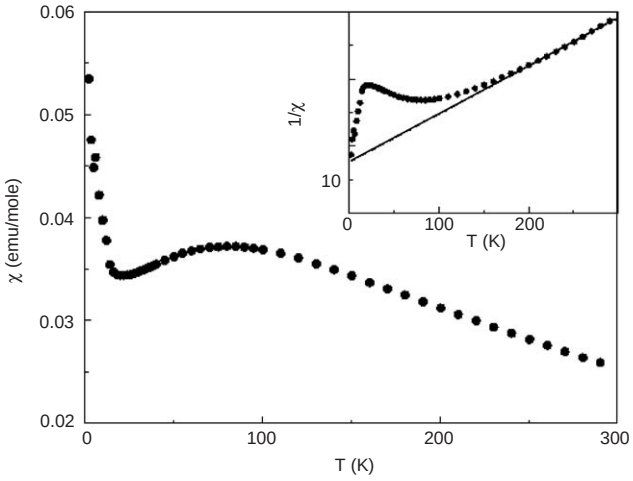

Fig. 7. Thermal variation of susceptibility for **I**. Inset shows the inverse susceptibility. The dashed line represent the Curie–Weiss fit of the high temperature data.

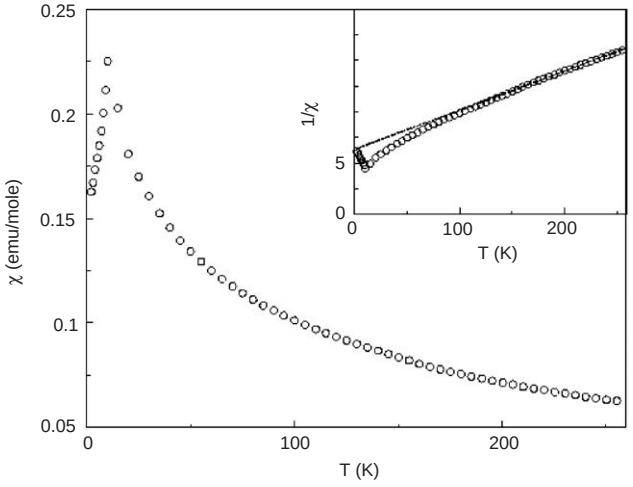

Fig. 8. Thermal variation of susceptibility for **II**. Inset shows the inverse susceptibility. The dashed line represent the Curie–Weiss fit of the high temperature data.

6. Conclusions

In summary, the syntheses and structures of two new iron phosphates, **I**, $[C_5N_2H_{14}]_2[Fe_2^{III}F_2(HPO_4)_4]\cdot 2H_2O$, **II**, and $[C_5N_2H_{14}][Fe_4^{III}(H_2O)_4F_2(PO_4)_4]$, have been accomplished using hydrothermal methods employing organic complexes as the source for iron. These and the earlier reported iron phosphate structures (7(b), 7(c))

clearly indicate the merits of using unusual complex precursors as the starting source for the metal ions. The iron atoms in both the compounds are in +3 oxidation state and have only anti-ferromagnetic interactions. The formation of **II** with two distinct building units, SBU-6 and SBU-2, is also noteworthy. This induces questions about the correlated influence of the kinetics and composition of the starting mixture on the nature of the SBU's both in the liquid and in the final solid. More such examples are required to be able to correlate these influences. We are presently working on the merits of using different inorganic coordination complexes of iron as the starting source for the synthesis of novel iron phosphates employing hydrothermal methods.

Acknowledgments

SN thanks the Department of Science and Technology (DST), Government of India for the award of a research grant and SM thanks the University Grants Commission (UGC) for the award of a research fellowship.

References

[1] P.B. Moore, Am. Miner. 55 (1970) 135.
[2] K.-H. Lii, Y.-F. Huang, V. Zima, C.-Y. Huang, H.-M. Lin, J.-C. Jiang, F.-L. Liao, S.L. Wang, Chem. Mater. 10 (1998) 2599 (and references therein).
[3] M. Cavellec, D. Riou, J.-M. Greneche, G. Ferey, Inorg. Chem. 36 (1997) 2187.
[4] V. Zima, K.-H. Lii, J. Chem. Soc. Dalton Trans. (1998) 4109.
[5] Z.A.D. Lethbridge, P. Lightfoot, R.E. Morris, D.S. Wragg, P.A. Wright, Å. Kvick, G. Vaughan, J. Solid State Chem. 142 (1999) 455.
[6] S. Mandal, S. Natarajan, W. Klein, M. Panthofer, M. Jansen, J. Solid State Chem. 173 (2003) 367.
[7] M. Cavellec, D. Riou, G. Ferey, J. Solid State Chem. 112 (1994) 441.
[8] M. Cavellec, D. Riou, G. Ferey, Eur. J. Solid State Inorg. Chem. 32 (1995) 271.
[9] M. Cavellec, D. Riou, G. Ferey, Acta Crystallogr. C 51 (1995) 2242.
[10] M.R. Cavellec, J.M. Greneche, D. Riou, G. Ferey, Chem. Mater. 10 (1998) 1914.
[11] J.R.D. DeBord, W.M. Reiff, R.C. Haushalter, J. Zubieta, J. Solid State Chem. 125 (1996) 186.
[12] K.-H. Lii, Y.-F. Huang, Chem. Commun. (1997) 1311.
[13] V. Zima, K-H. Lii, N. Nguyen, A. Ducouret, Chem. Mater. 10 (1998) 1914.
[14] A. Mgaidi, H. Boughzala, A. Driss, R. Clerac, C. Coulon, J. Solid State Chem. 144 (1999) 163.
[15] A.R. Cowley, A.M. Chippindale, J. Chem. Soc. Dalton Trans. (2000) 3425.
[16] A. Choudhury, S. Natarajan, C.N.R. Rao, Chem. Commun. (1999) 1305.
[17] A. Choudhury, S. Natarajan, Int. J. Inorg. Chem. 2 (2000) 217.
[18] A. Choudhry, S. Natarajan, J. Solid State Chem. 154 (2000) 507.
[19] S. Mahesh, M.A. Green, S. Natarajan, J. Solid State Chem. 165 (2002) 334.
[20] M. Cavellec, D. Riou, G. Ferey, Inorg. Chim. Acta 291 (1999) 317.
[21] T. Loiseau, G. Ferey, J. Chem. Soc., Chem. Commun. (1992) 1197.
[22] M. Cavellec, D. Riou, C. Ninclaus, J.-M. Greneche, G. Ferey, Zeolites 17 (1996) 250.
[23] M. Cavellec, D. Riou, J.-M. Greneche, G. Ferey, J. Magn. Magn. Mater. 163 (1996) 173.
[24] M. Cavellec, C. Egger, J. Linares, M. Nogues, F. Varret, G. Ferey, J. Solid State Chem. 134 (1997) 349.
[25] M. Cavellec, J.-M. Greneche, D. Riou, G. Ferey, Microporous Mater. 8 (1997) 103.
[26] M. Cavellec, J.-M. Greneche, G. Ferey, Microporous Mesoporous Mater. 20 (1998) 45.
[27] K.-H. Lii, Y.-F. Huang, Chem. Commun. (1997) 839.
[28] K.-H. Lii, Y-F. Huang, J. Chem. Soc. Dalton Trans. (1997) 2221.
[29] C.-Y. Huanh, S.-L. Wang, K.-H. Lii, J. Porous Mater. 5 (1998) 147.
[30] V. Zima, K.-H. Lii, J. Solid State Chem. 139 (1998) 326.
[31] J.R.D. DeBord, W.M. Reiff, C.J. Warren, R.C. Haushalter, J. Zubieta, Chem. Mater. 9 (1997) 1994.
[32] S. Neeraj, S. Natarajan, Int. J. Inorg. Mater. 1 (1999) 317.
[33] F.C. Hawthorne, Acta Crystallogr. Sect. B 50 (1994) 481 (and references therein).
[34] G.M. Sheldrick, SADABS Siemens Area Detector Absorption Correction Program, University of Conttingen, Gottingen, Germany.
[35] G.M. Sheldrick, SHELXTL-PLUS Program for Crystal Structure Solution and Refinement, University of Gottingen, Gottingen, Germany.
[36] I.D. Brown, D. Altermatt, Acta Crystallogr. Sect. B 41 (1984) 244.
[37] G. Ferey, J. Fluorine Chem. 72 (1995) 187.
[38] G. Ferey, C.R. Acad. Sci. Ser. II, (1998) 1.
[39] G. Ferey, J. Solid State Chem. 152 (2000) 37.
[40] G. Ferey, Chem. Mater. 13 (2001) 3084.
[41] M.R. Cavellec, D. Riou, G. Gerey, Inorg. Chim. Acta 291 (1999) 317 (and the references therein).
[42] K. Abu-Shandi, H. Winkler, M. Gerden, F. Emmerling, B. Wu, C. Janiak, Dalton Trans. (2003) 2815.
[43] R.A. Ramik, B.D. Sturman, P.J. Dunn, A.S. Poverennykh, Can. Mineral. 18 (1980) 185.
[44] T. Loiseau, F. Serpaggi, G. Ferey, Chem. Commun. (1997) 1093.
[45] M.P. Attfield, R.E. Morris, I. Burshtein, C.F. Campana, A.K. Cheetham, J. Solid State Chem. 118 (1995) 412.